Eur. Phys. J. B **1**, 453–464 (1998)

THE EUROPEAN PHYSICAL JOURNAL B

Ionic diffusion on a lattice: Effects of the order-disorder transition on the dynamics of non-equilibrium systems

R. Nassif[1], Y. Boughaleb[1], A. Hekkouri[1], J.F. Gouyet[2,a], and M. Kolb[2,3]

[1] Laboratoire de Physique de la Matière Condensée, Université Hassan II, Faculté des Sciences Ben M'Sik, Casablanca, Morocco
[2] Laboratoire de Physique de la Matière Condensée, École Polytechnique, 91128 Palaiseau, France
[3] Laboratoire de Chimie Théorique, École Normale Supérieure, 69364 Lyon, France

Received: 26 June 1997 / Revised: 18 September 1997 / Accepted: 10 November 1997

Abstract. We examine the behaviour of the concentration profiles of particles with repulsive interactions diffusing on a host lattice. At low temperature, the diffusion process is strongly influenced by the presence of ordered domains. We use mean field equations and Monte-Carlo simulations to describe the various effects which influence the kinetic behaviour. An effective diffusion coefficient is determined analytically and is compared with the simulations. Finite gradient effects on the ordered domains and on the diffusion are discussed. The kinetics studied is relevant for superionic conductors, for intercalation and also for the diffusion of particles adsorbed on a substrate.

PACS. 05.50.+q Lattice theory and statistics: Ising problems – 05.60.+w Transport processes theory – 68.35.Fx Diffusion; interface formation

1 Introduction

Transport in superionic conductors [1], ionic intercalation [2] or diffusion of adsorbed atoms on surfaces [3,4] are phenomena which can frequently be modelled, in a first approximation, as a distribution of particles evolving in a periodic potential, either through a host lattice or on a substrate.

Much research effort has been devoted to the study of the general aspects of the dynamics of first-order phase transition in non-equilibrium systems [5]. In the case of repulsive interactions, the transitions are order-disorder transitions with the appearance of order on sublattices. In non- equilibrium systems, where the concentration is non-homogeneous, the diffusion processes will be complicated by the appearance of these ordered domains, in a certain concentration range. Only a few studies [6–9,3] have been devoted to this behaviour, in spite of its impact on intercalation, surface diffusion and interdiffusion problems.

During the last ten years the behaviour of intercalation processes in superionic conductors have attracted much interest both experimentally and theoretically (see for example Ref. [1]). During intercalation, the ions diffuse in the periodic potential of the host lattice. This lattice does not in general remain inactive: deformations lead to various physical complications of the intercalation process (effective anisotropic long-range coupling between the diffusive ions, coupling between neighbouring layers *etc.*). In addition, the diffusion process is not always in a hopping regime and a fluid like approach may be more appropriate [10].

A closely related phenomenon is the surface diffusion of adsorbates, which diffuse in the periodic potential of the surface. This phenomenon is important in relation with catalysis, corrosion and crystal growth problems. In these situations, the diffusion process is also influenced by the presence of ordered regions [4].

Here we will only consider systems that can be well described by a hopping regime. In a hopping regime, even in presence of interactions, the barriers that the particles have to overcome are always much higher than the thermal energy of the particle [11]. This is the case for instance for lithium intercalated titanium diselenide [12], or for lithium-aluminium systems [13], at not too high temperatures.

The understanding of the formation of ordered states and the non-linear diffusion on a lattice in the presence of repulsive interactions progressed considerably at the beginning of the seventies when Sato and Kikuchi applied their Path Probability Method to β-alumina solid electrolytes [14]. Applications and numerical verifications of this method were given by Murch and Murch and Thorn [15]. In this study, the Coulomb repulsive interaction between the ions is supposed to be screened in such a way that the remaining interaction is short-range: in practice only nearest neighbour repulsive interactions have been taken into account.

[a] e-mail: jean-françois.gouyet@polytechnique.fr

Other methods were also developed, in particular to understand tracer diffusion. Being perturbative or self-consistent methods, they are in general limited to low or high concentrations of diffusing particles, the intermediate case (where phase transitions appear) being very difficult to study. A review can be found in reference [16].

At the same time, Monte-Carlo simulations have been performed. Natori *et al.* [6] studied the diffusion of repulsive particles which generates ordered structures at low enough temperature. Sadiq and Binder [7] performed Monte-Carlo simulations of the same problem, but with a symmetrical "Kawasaki dynamics", they showed clearly that the system evolves towards an ordered state. In such a model the collective diffusion coefficient is symmetrical with respect to a particle- vacancy exchange.

The purpose of the present paper is to examine in more detail the behaviour of particles with repulsive nearest neighbour interactions diffusing in a periodic and fixed host lattice, out of equilibrium and in the hopping regime. The aim is not only to determine the effect of ordered regions, but also to examine the effect of finite concentration gradients as they appear in the dynamics of non homogeneous systems. We use primarily a mean field approximation and will compare the results with data from Monte-Carlo simulations. The paper is organized as follows: in Section 2, we present the Monte-Carlo calculations of the diffusing particles on a square lattice from which we determine an effective diffusion coefficient; in Section 3, we recall the main features of the lattice gas model, introduce the mean-field approximation and the idea of simultaneously evolving sublattices and we state the main results of the order-disorder transition at equilibrium; in Section 4, we examine the out-of-equilibrium order-disorder dynamics in the framework of our mean-field approximation. Finally, Section 5 is devoted to a comparison between Monte-Carlo calculation and mean-field scaling results and to the discussion.

2 Monte-Carlo calculations

The most direct investigation of the evolution of the average concentration profile and of the ordering at low temperature is by Monte-Carlo simulations [9,15]. Therefore we first present the results obtained from the dynamical evolution towards equilibrium of an initially inhomogeneous lattice gas. We consider a square lattice which is semi-infinite in one direction, the diffusion direction (x- or horizontal direction) and which is finite and periodically bounded in the other (y- or vertical direction). At time $t = 0$, the lattice is empty, except for the $x = 0$ row, whose concentration is maintained fixed and equal to 1 at all times. Defining $p(\mathbf{x}, t)$ as the probability to find a particle at site $\mathbf{x}$ at time t, one has $\{p(x = 0, y, t) \equiv 1, p(x > 0, y, t = 0) \equiv 0\}$. In the simulations, $p(\mathbf{x}, t)$ is the occupation at site $\mathbf{x} = (x, y)$, averaged over many realizations. For $t > 0$, the particles diffuse freely into the $x > 0$ plane, and we will calculate the concentration $p(x, t)$ as a function of x and t, averaged over all y.

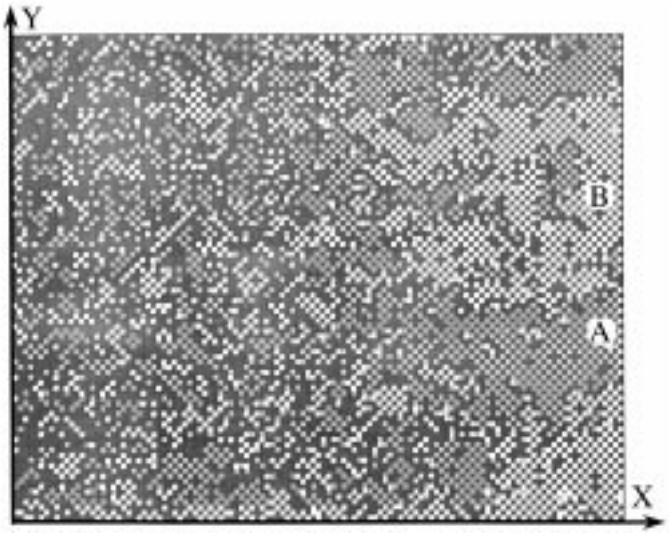

Fig. 1. Monte-Carlo calculation of the domain formation on the square lattice due to the repulsive interaction below the critical temperature. A window of average concentrations between $p = 0.75$ and $p = 0.5$ along the x-axis is shown. Two types of domains (A respectively B) form around $p \cong 0.5$, corresponding to the occupation of the two sublattices.

Instead of the open boundary conditions one may also consider stationary non-equilibrium states with finite fixed boundaries in the x-direction: $\{p(x = 0, t) \equiv 1\}$ and $\{p(x = L, t) \equiv 0\}$. Such a system in principle has the advantage that the effective diffusion coefficient D_{eff} can be obtained directly from the stationary concentration profile. One expects that the results do not depend on the boundary condition in the limit of small gradients respectively large L. The following equation describes the average density,

$$\frac{\partial p(\mathbf{x}, t)}{\partial t} = \text{div}(D_{\text{eff}}(p)\mathbf{grad}\ p) \equiv 0 = \frac{\partial}{\partial x} D_{\text{eff}}(p) \frac{\partial p}{\partial x} \quad (1)$$

which, for fixed boundary conditions, yields

$$D_{\text{eff}}(p) = \frac{-j_0}{\partial p/\partial x} \quad (2)$$

where j_0 is the stationary current in the system. Because of the (physically motivated) hopping rate, $w(\{n\}) = w_0 \mathrm{e}^{-\varepsilon \sum_i n_i/kT}$, where $n_i = 0, 1$ is the occupation number and the sum is over nearest neighbour sites, the gradient in the intermediate concentration range is rather large and therefore the data of the simulations are quite noisy (for the chosen form of $w(\{n\})$ an isolated vacancy diffuses much faster than an isolated particle). Therefore the diffusion coefficient D_{eff} can be determined more reliably from simulations with semi-infinite boundaries.

Below the critical temperature (the actual simulations were performed at $T = 0.88 T_{\text{c}}$) we observe, as expected, the appearance of ordered regions. A typical structure is shown in Figure 1, where an actual configuration between a concentration $p = 0.75$ at the left and $p = 0.5$ at the right is represented. The progressive appearance

of the two kinds of ordered domains A and B near $p \cong 0.5$ is clearly visible. These domains, due to the nearest neighbour repulsion, correspond to the black, respectively white, squares of a chessboard. Figure 2, shows the evolution of the concentration profile, below the critical temperature (here $\varepsilon/kT = -2.0$; the corresponding critical temperature is $\varepsilon/kT_c = -1.76$), for various times ranging from 256 MCS to 32768 MCS (one Monte-Carlo step, MCS, corresponds to one diffusion trial per particle). In contrast with the case of attractive interactions where the diffusion coefficient becomes negative in the miscibility gap and a 4th-order differential master equation needs to be considered, for the case of repulsive interactions the usual diffusion equation for each of the sublattices and with an effective diffusion coefficient adequately describes the asymptotic large time evolution. As a consequence we expect scaling of the concentration profiles with the reduced coordinate $x/\sqrt{t}$. This is verified in Figure 3, where one can see that for large times the profiles collapse into a single scaling form when plotted against the scaling variable. This result will be compared with the mean-field approach below. It is also possible to extract the order parameter as a function of the concentration from the Monte-Carlo data. The order parameter is defined as the difference between the average concentration on the sublattices A and B:

$$\eta = \frac{p^{\mathrm{A}}(x) - p^{\mathrm{B}}(x)}{2}$$

(the average concentration p, being in this case $(p^{\mathrm{A}}(x) + p^{\mathrm{B}}(x))/2$).

In Figure 4, we show the $\eta(p)$ curves extracted from the Monte-Carlo calculations, at three different times in the simulations (they are calculated from the absolute value of the difference of the sublattice magnetization over small domains of size 2×2 to 16×16, for a given x and averaged over y). At large enough times the curve tends towards an invariant profile. Notice that $\eta(p)$ vanishes smoothly around $p \cong 0.4$ and $p \cong 0.6$, in contrast with the equilibrium phase diagram, for which $\eta(p)$ vanishes in a singular fashion (a more detailed discussion is given in Sect. 4.2 below). This is due to finite gradient and finite time effects as well as due to the finite domain averaging used to determine $\eta(p)$ in the simulations. An effective diffusion coefficient D_{eff} can be determined from the Monte-Carlo calculations in different way. We may use Fick's law and calculate the average current between successive rows; this method is rather noisy. A second approach supposes that the asymptotic scaling behaviour has been reached, and that the Boltzmann equation [17] for diffusing particles is valid. This equation is obtained by substituting $p(u)$ with $u = x/\sqrt{t}$ for $p(x,t)$ in the diffusion equation. We are then led to a Boltzmann-Matano [17,18] type of analysis. A simple calculation gives

$$D_{\mathrm{eff}} = -\frac{up(u) + \int_u^\infty p(u)du}{2\mathrm{d}p/\mathrm{d}u} \qquad (3)$$

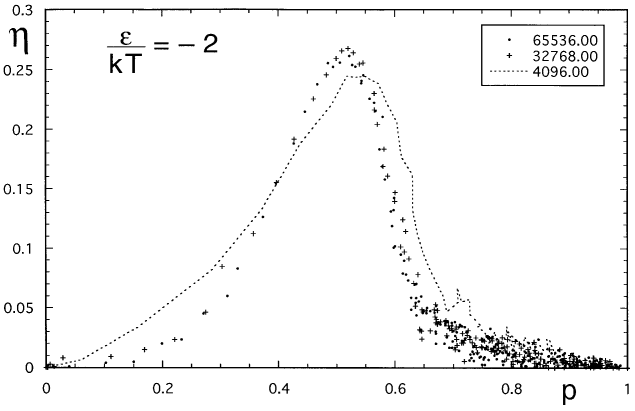

Fig. 4. Order parameter η (difference of sublattice magnetization) as a function of p from Monte-Carlo simulations. $\eta \neq 0$ in the range between $p \cong 0.3$ and $p \cong 0.6$. The transitions rounded by finite gradient respectively finite time effects.

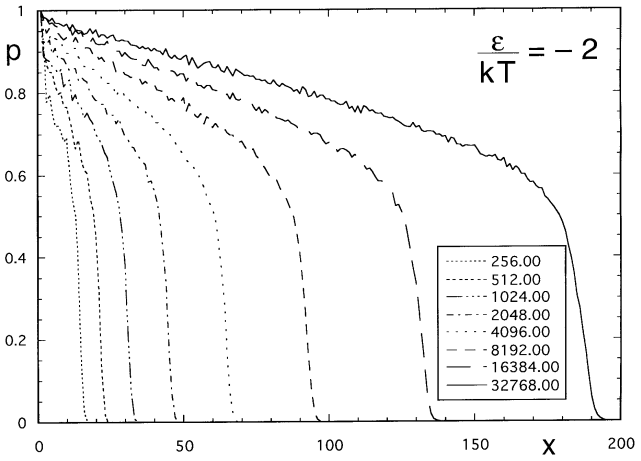

Fig. 2. Average concentration profiles $p(x)$ from Monte-Carlo simulations for diffusion with repulsive interaction ($T/T_c = 0.88$) for a semi-infinite system at different times indicated in the inset.

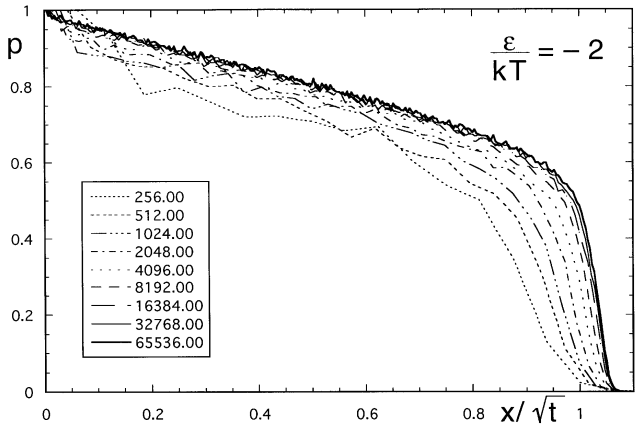

Fig. 3. Same data as in Figure 2, now plotted in scaled form: p *vs.* $x/\sqrt{t}$. For large times all the profiles collapse on a unique master curve.

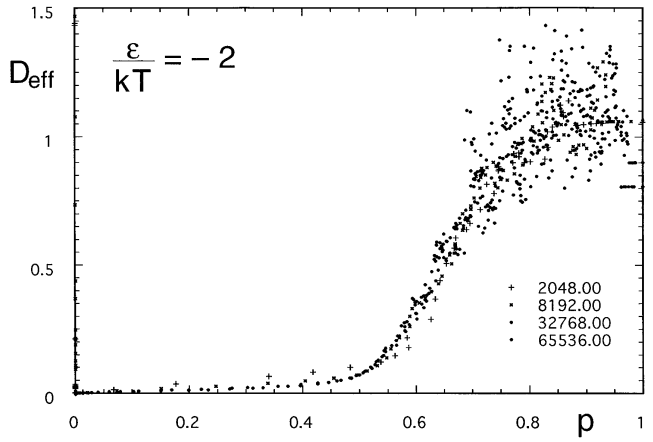

Fig. 5. Diffusion coefficient as a function of p, measured from Monte-Carlo simulations at $T/T_c = 0.88$, for different successive times. Due to the repulsive interaction, $D_{\rm eff}$ increases when p increases, except possibly close to $p = 1$ where the vacancies availability goes to zero.

which can be determined directly from the numerical calculations. The results for various times at a temperature given by $\varepsilon/kT = -2$ ($T = 0.88T_c$) are shown in Figure 5. The diffusion coefficient has been normalized such that $D_{\rm eff} = 1$ for $p = 1$. Below, we will compare these results with the results from the mean field approach in the lattice gas model.

3 The lattice gas model, a mean-field analytical approach

The master equation which describes how a general configuration $\{n\} = \{n_1, n_2, \ldots n_i, n_j, \ldots n_N\}$ evolves with time can be written as,

$$\frac{\partial}{\partial t}P(\{n\},t) = \sum_{\{n'\}}\{W(\{n'\}\to\{n\})P(\{n'\},t) - W(\{n\}\to\{n'\})P(\{n\},t)\} \quad (4)$$

where $P(\{n\},t)$ is the probability to find the configuration $\{n\}$ at time t, and $W(\{n'\}\to\{n\})$ is the transition rate from $\{n'\}$ to $\{n\}$ and is defined by

$$W(\{n'\}\to\{n\}) = = \sum_{i,j} w_{ij}(\{n\})n'_i(1-n'_j)\delta_{n_j\ n'_i}\delta_{n_i\ n'_j}\delta^{i,j}_{\{n\}\{n'\}} \quad (5)$$

where w_{ij} is the jump probability from site i to site j, which depends on the particle environment; the term $n_i(1-n_j)$ where $n_i = 0, 1$ assures that site i is occupied while site j must be empty; this term expresses the fact that double occupation is forbidden. An operator n_i with $\mathrm{n}_i|\{n'\}\rangle = n'_i|\{n'\}\rangle$ may be conveniently introduced.

If we are only interested in the evolution of the average concentration $p_k \equiv \langle \mathrm{n}_k\rangle$ at site k, equation (4) reduces to

$$\frac{\partial p_k}{\partial t} \equiv \frac{\partial}{\partial t}\langle \mathrm{n}_k\rangle \equiv \frac{\partial}{\partial t}\sum_{\{n'\}} n_k P(\{n\},t) = \sum_j \langle \mathrm{w}_{jk}(\{\mathrm{n}\})\mathrm{n}_j(1-\mathrm{n}_k) - \mathrm{w}_{kj}(\{\mathrm{n}\}\mathrm{n}_k(1-\mathrm{n}_j)\rangle. \quad (6)$$

For simplicity, the jumps are supposed to be limited to nearest neighbour sites $k + a'$ of any site k. It is then convenient to introduce a current operator $\mathcal{J}_{k,k+a}(\{\mathrm{n}\})$ along the link $k \to k + a$, so that equation (6) becomes, taking $j = k + a$,

$$\frac{\partial p_k}{\partial t} = -\sum_a \langle \mathcal{J}_{k,k+a}(\{\mathrm{n}\})\rangle \quad (7)$$

where the average current in the bond (i, j) is

$$J_{ij}(\{p\}) \equiv \langle \mathcal{J}_{ij}(\{\mathrm{n}\}\rangle = \langle \mathrm{w}_{ij}\mathrm{n}_i(1-\mathrm{n}_j) - \mathrm{w}_{ji}\mathrm{n}_j(1-\mathrm{n}_i)\rangle. \quad (8)$$

Equation (7) is nothing but the discrete version of the conservation law $\partial p/\partial t = \mathrm{div}J$.

Here we are interested in lattice gases with repulsive interactions for which an order-disorder transition appears at some critical temperature T_c. As indicated above, on the square and simple cubic lattice there is symmetry breaking with respect to two interlaced sublattices {A} and {B}; they will be distinguished by their "colour" A and B (as in Fig. 1). The occupation probabilities p on these sublattices will be identified by an upper index A or B, $p_i^{\rm A}$ and $p_j^{\rm B}$ with $i \in \{\mathrm{A}\}$ and $j \in \{\mathrm{B}\}$; k will designate any site i or j. Equations (7,8) then become

$$\frac{\partial p_i^{\rm A}}{\partial t} = -\sum_{j=i+a}\langle \mathcal{J}_{ij}^{\rm AB}(\{\mathrm{n}\})\rangle, \frac{\partial p_j^{\rm B}}{\partial t} = -\sum_{i=j+a}\langle \mathcal{J}_{ji}^{\rm BA}(\{\mathrm{n}\})\rangle \quad (9)$$

with a current defined by

$$J_{ij}^{\rm AB} \equiv \langle \mathcal{J}_{ij}^{\rm AB}(\{\mathrm{n}\})\rangle = \langle \mathrm{w}_{ij}^{\rm AB}\mathrm{n}_i^{\rm A}(1-\mathrm{n}_j^{\rm B}) - \mathrm{w}_{ji}^{\rm BA}\mathrm{n}_j^{\rm B}(1-\mathrm{n}_i^{\rm A})\rangle. \quad (10)$$

3.1 The simultaneously evolving sublattices

As the designation of the colours A and B is arbitrary, it is very convenient to consider the two sublattices for each site k simultaneously: the A sublattice on the 'white' sites (of the chessboard) are coupled to the B sublattice on the 'black' sites and similarly the B sublattice on the 'white' sites are coupled to the A sublattice on the 'black' sites. Both evolve independently from one another. If the initial configurations of the two sets of coupled sublattices are chosen very close to each other and to a constant value, and if they evolve together in parallel, the concentration $p_k^{\rm A}$ for the A- and $p_k^{\rm B}$ for the B-sublattice on *each* site k

behaves smoothly at all times. This is indeed confirmed numerically: p_k^α and p_{k+a}^α ($\alpha = $ A or B) remain close; this can be interpreted as the fact that no chaotic regime appears. The properties of such "Simultaneously Evolving Sublattices" (SES) have been detailed elsewhere [19]. SES greatly simplifies the analytic expressions that we now develop.

The choice of the averaging procedure for the mean-field treatment can be motivated by physical or by practical (*i.e.* computational) considerations. It will be chosen in such a way that it is as close as possible to the usual thermodynamic approach (case I of Ref. [20]). In a first step the average in equation (10) is reduced to the form,

$$J_{ij}^{\mathrm{AB}}(\{p\}) = \langle \tilde{\mathrm{w}}_{ij}^{\mathrm{AB}} \rangle p_i^{\mathrm{A}}(1-p_j^{\mathrm{B}}) - \langle \tilde{\mathrm{w}}_{ji}^{\mathrm{BA}} \rangle p_j^{\mathrm{B}}(1-p_i^{\mathrm{A}}) \quad (11)$$

where there still remains some arbitrariness in how the average of $\mathrm{w}_{ij}(\{\mathrm{n}\})$ is taken. We will use this arbitrariness to agree with well established thermodynamics.

In most applications, the host potential in which the hopping particles diffuse can be seen as an "egg-box" potential. The associated lattice is the lattice of the potential minima. The bonds join nearest neighbor sites through a saddle point. The jump probabilities $\mathrm{w}_{ij}(\{\mathrm{n}\})$ for a lattice gas hopping model (Eyring absolute regime) are then essentially functions of the energy difference between its initial well (site k) and the saddle point (in-between k and $k+a$), as seen by the jumping particle. Here we consider only a nearest neighbour interaction and the saddle point is supposed at fixed (zero) energy, hence not sensitive to the occupation of the neighbouring sites. The Hamiltonian of the system of diffusing particles for a given configuration $\{n\}$ (in the hopping model, the particles spend most of their time in the wells) is,

$$\mathcal{H} = -\sum_{i,j} \varepsilon_{ij}^{\mathrm{AB}} \mathrm{n}_i^{\mathrm{A}} \mathrm{n}_j^{\mathrm{B}} - \sum_i \varepsilon_i^{\mathrm{A}} \mathrm{n}_i^{\mathrm{A}} - \sum_j \varepsilon_j^{\mathrm{B}} \mathrm{n}_j^{\mathrm{B}}. \quad (12)$$

For a short range-repulsive interaction we have, $\varepsilon_{ij} = \varepsilon < 0$ when $\{i,j\}$ are nearest neighbours, and zero otherwise. Furthermore we will choose $\varepsilon_i^{\mathrm{A}} = \varepsilon_j^{\mathrm{B}} = \mu_{\mathrm{e}}$, which corresponds to a uniform lattice where all the sites are equivalent. With these conditions, the standard jump operator at temperature T, which leads to Arrhenius jump probabilities and Boltzmann equilibrium distribution, is a

$$\mathrm{w}_{ik}^{\mathrm{AB}}(\{\mathrm{n}\}) = w_0 \exp - \frac{\varepsilon}{kT} \sum_{a' \neq k-i} \mathrm{n}_{i+a'}^{\mathrm{B}} \quad (13a)$$

($w_0^{\mathrm{A}} = w_0^{\mathrm{B}} = w_0$ on a uniform lattice, is the jump probability of an isolated particle, and the final site is considered empty in the expression of w).

The jump probability operator can also be written in a different way [20],

$$\tilde{\mathrm{w}}_{ik}^{\mathrm{AB}}(\{\mathrm{n}\}) = w_0 \exp - \left(s \frac{\varepsilon}{kT} \mathrm{n}_k^{\mathrm{B}} \right) \exp \left(- \frac{\varepsilon}{kT} \sum_{a'} \mathrm{n}_{i+a'}^{\mathrm{B}} \right) \quad (13b)$$

which is equivalent to (13a), due to the fact that the final site is empty ($(1-n_k)$ term in (6)). We will choose here the parameter s equal to zero, to agree with usual thermodynamics.

3.2 Mean-field approach

When all the operators n_k in the expressions for the jump probabilities $w_{k,k+a}$ have been replaced by their average concentrations p_k (see Appendix A), it is possible to write the current in a simple form, reminiscent of a Cahn-Hilliard equation. The current may be written as a function of the discrete gradient of the activities C_k:

$$J_{ij}^{\mathrm{AB}}(\{p\}) = -S_{ij}^{\mathrm{AB}}(C_j^{\mathrm{B}} - C_i^{\mathrm{A}}) \quad (14)$$

or equivalently as a function of the chemical potentials:

$$J_{ij}^{\mathrm{AB}}(\{p\}) = -M_{ij}^{\mathrm{AB}}(\mu_j^{\mathrm{B}} - \mu_i^{\mathrm{A}}) \quad (15)$$

where

$$\begin{aligned} \mu_k^{\mathrm{A}} &= kT \log C_k^{\mathrm{A}} \\ &= -z\varepsilon(p_k^{\mathrm{B}} - \frac{1}{2}) - \varepsilon \sum_{a'} \mathcal{D}_{a'} p_k^{\mathrm{B}} + kT \log \frac{p_k^{\mathrm{A}}}{1-p_k^{\mathrm{A}}} \end{aligned} \quad (16)$$

and a similar relation for μ^{B} by permutation of A and B. $\mathcal{D}_a$ is a difference operator, defined by,

$$\mathcal{D}_a f(k) = f(k+a) - f(k).$$

The sum over a' in (16) is then a discrete Laplacian operator. M^{AB} is the associated mobility, which not only depends on the average concentration, but also on local concentration gradients.

3.3 The order-disorder transition

It is very easy to determine the phase diagram of the order-disorder transition in the mean-field approximation, from the above expressions. We need it here as a basis for the dynamics. This simple mean-field approximation leads only to a qualitatively correct phase diagram. A better mean-field approach would consist in using the pair approximation such as the Kikuchi cluster variation method [14], or the real space renormalization group [21] (in calculating phase diagrams, the cluster variation method is frequently more accurate than real space renormalization, except may be very close to the critical temperature), while the best results can in principle be obtained *via* Monte-Carlo methods [22]. But it is not the purpose here to improve the results on statics.

In Appendix B we recall the main features of the mean-field phase diagram. The phase diagram corresponding to the value $s = 0$, in equation (13b), is shown in Figure 6. The equilibrium relation between temperature kT, concentration p, and order parameter η is given by,

$$kT(p,\eta) = -\frac{2\varepsilon z \eta}{\log \left(1 - \dfrac{2\eta}{(p-\frac{1}{2})^2 - (\eta - \frac{1}{2})^2} \right)} \cdot \quad (17)$$

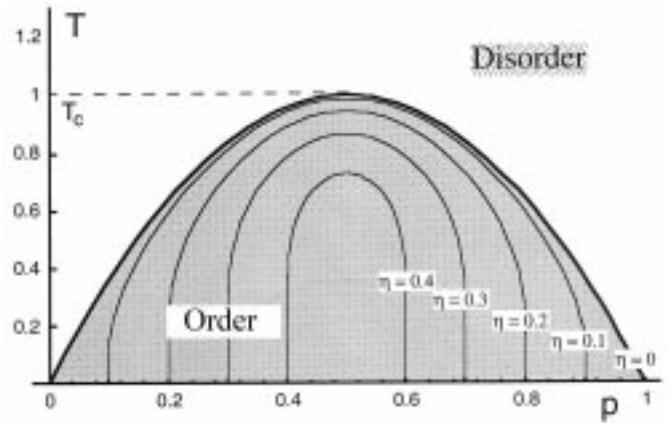

Fig. 6. Phase diagram of the order-disorder transition on the square lattice as a function of p, in mean field approximation.

4 The order-disorder dynamics

We have now all the elements to examine the dynamics of ionic diffusion in presence of an order-disorder transition in the intermediate concentration range. This dynamics has been simulated using the mean-field equations established above, to be compared with the Monte-Carlo results.

The mean concentration $\sum_k \langle p_k \rangle$ over a fixed domain of the lattice is a *conserved quantity*. From equations (7, 14), we see that the equation of evolution of the mean concentration p_k is [23],

$$\frac{\partial p_k}{\partial t} = \frac{1}{2} \sum_j \left\{ S_{kj}^{\mathrm{AB}} (C_j^{\mathrm{B}} - C_k^{\mathrm{A}}) + S_{kj}^{\mathrm{BA}} (C_j^{\mathrm{A}} - C_k^{\mathrm{B}}) \right\}. \quad (18)$$

In the case of a *centrosymmetric lattice* with nearest neighbours jumps, the evolution equation of p_k can be written as a discrete divergence of a current (conservation equation):

$$\frac{\partial p_k}{\partial t} = -\frac{1}{2} \sum_a \mathcal{D}_a J_{k-a,k}^{\mathrm{AB}}. \quad (18a)$$

On the other hand, the order parameter η_k is a *nonconserved quantity*, with an equation of motion given by,

$$\frac{\partial \eta_k}{\partial t} = \frac{1}{2} \sum_j \left\{ S_{kj}^{\mathrm{AB}} (C_j^{\mathrm{B}} - C_k^{\mathrm{A}}) - S_{kj}^{\mathrm{BA}} (C_j^{\mathrm{A}} - C_k^{\mathrm{B}}) \right\}. \quad (19)$$

It is possible to simplify equations (18) and because of the repulsive interactions to restrict the expansion in the kinetic equations to second order in the intersite distance a (to second spatial derivatives in the continuous case) for slow variations of the concentrations, *i.e.* at large times. For the evolution of the average concentration on a centrosymmetric lattice we then obtain

$$\frac{\partial p_k}{\partial t} = -\frac{1}{2} \sum_a \mathcal{D}_{-a} \left\{ D(p_k, \eta_k) \mathcal{D}_a p_k + E(p_k, \eta_k) \mathcal{D}_a \eta_k \right\} \quad (20)$$

where,

$$D(p_k, \eta_k) = \frac{1}{2} \left\{ w^{\mathrm{BA}}(k) + w^{\mathrm{AB}}(k) - Kz(j_0^{\mathrm{A}}(k) + j_0^{\mathrm{B}}(k)) \right\}$$
$$E(p_k, \eta_k) = \frac{1}{2} \left\{ w^{\mathrm{BA}}(k) + w^{\mathrm{AB}}(k) + Kz(j_0^{\mathrm{A}}(k) - j_0^{\mathrm{B}}(k)) \right\} \quad (20a)$$

with,

$$\begin{aligned} w^{\mathrm{AB}}(k) &= w^{\mathrm{A}}(k) p_k^{\mathrm{A}} + w^{\mathrm{B}}(k)(1 - p_k^{\mathrm{A}}) \\ w^{\mathrm{BA}}(k) &= w^{\mathrm{B}}(k) p_k^{\mathrm{B}} + w^{\mathrm{A}}(k)(1 - p_k^{\mathrm{B}}) \\ w^{\mathrm{A}}(k) &= w_0 \exp(-Kz p_k^{\mathrm{B}}) \\ w^{\mathrm{B}}(k) &= w_0 \exp(-Kz p_k^{\mathrm{A}}) \\ j_0^{\mathrm{A}}(k) &= w^{\mathrm{A}}(k) p_k^{\mathrm{A}} (1 - p_k^{\mathrm{B}}) \\ j_0^{\mathrm{B}}(k) &= w^{\mathrm{B}}(k) p_k^{\mathrm{B}} (1 - p_k^{\mathrm{A}}); K = \varepsilon / kT. \end{aligned} \quad (20b)$$

The lack of a conservation law leads to more complicated relations for $\partial \eta_k / \partial t$.

$$\begin{aligned} \frac{\partial \eta_k}{\partial t} =& - z \left(j_0^{\mathrm{A}}(k) - j_0^{\mathrm{B}}(k) \right) + F(p_k, \eta_k) \Delta_a p_k \\ &+ G(p_k, \eta_k) \Delta_a \eta_k + \frac{1}{2} \Bigg\{ P(p_k, \eta_k) \sum_a (\mathcal{D}_a p_k)^2 \\ &+ Q(p_k, \eta_k) \sum_a \mathcal{D}_a p_k \mathcal{D}_a \eta_k + R(p_k, \eta_k) \sum_a (\mathcal{D}_a \eta_k)^2 \Bigg\} \end{aligned} \quad (21)$$

where,

$$\begin{aligned} F(p_k, \eta_k) &= \frac{1}{2} \left\{ w^{\mathrm{AB}}(k) - w^{\mathrm{BA}}(k) + 3Kz(j_0^{\mathrm{A}}(k) - j_0^{\mathrm{B}}(k)) \right\} \\ G(p_k, \eta_k) &= -\frac{1}{2} \left\{ w^{\mathrm{AB}}(k) - w^{\mathrm{BA}}(k) + 3Kz(j_0^{\mathrm{A}}(k) - j_0^{\mathrm{B}}(k)) \right\} \\ P(p_k, \eta_k) &= Kz\{(1 - p^{\mathrm{B}}(k)) w^{\mathrm{A}}(k) - (1 - p^{\mathrm{A}}(k)) w^{\mathrm{B}}(k)\} \\ &\quad - \frac{K^2 z^2}{2} (j_0^{\mathrm{A}}(k) - j_0^{\mathrm{B}}(k)) \\ Q(p_k, \eta_k) &= K^2 z^2 (j_0^{\mathrm{A}}(k) + j_0^{\mathrm{B}}(k)) \\ R(p_k, \eta_k) &= -Kz\{(1 - p^{\mathrm{B}}(k)) w^{\mathrm{A}}(k) - (1 - p^{\mathrm{A}}(k)) w^{\mathrm{B}}(k)\} \\ &\quad - \frac{K^2 z^2}{2} (j_0^{\mathrm{A}}(k) - j_0^{\mathrm{B}}(k)) \end{aligned} \quad (21a)$$

while Δ_a is a discrete Laplacian: $\frac{1}{2} \sum_a \mathcal{D}_{-a} \mathcal{D}_a$. Notice that $\eta(k,t) = 0$ is always a solution, but it becomes unstable in the coexistence region. This can be seen in equation (21) in which $p^{\mathrm{A}}(k) = p^{\mathrm{B}}(k)$ gives $j_0^{\mathrm{A}} = j_0^{\mathrm{B}} = 0$, $F = 0$ and $P = 0$.

4.1 Large time diffusion equation

We now consider the stable solutions. The important point here is that due to the zeroth term order $(j_0^{\mathrm{A}} - j_0^{\mathrm{B}})$, η_k rapidly relaxes to its equilibrium value: at late times, when the local distribution becomes relatively homogeneous, all

the gradients may be neglected and $j_0^{\rm A}(k) = j_0^{\rm B}(k)$ from (21) and $\eta_k \approx \eta_{\rm eq}(p_{\rm k}, T)$ defined implicitly by equation (17).

Equation (20) then leads to a simplified equation for the local concentration,

$$\frac{\partial p_k}{\partial t} = -\frac{1}{2}\sum_a \mathcal{D}_{-a}\left\{\left[D(p_k,\eta_{\rm eq}) + E(p_k,\eta_{\rm eq})\frac{\partial \eta_{\rm eq}}{\partial p_k}\right]\mathcal{D}_a p_k\right\}. \tag{22}$$

This equation is a simple diffusion equation, with an effective concentration dependent diffusion coefficient,

$$D_{\rm eff}(p_k) = D(p_k,\eta_{\rm eq}) + E(p_k,\eta_{\rm eq})\frac{\partial \eta_{\rm eq}}{\partial p_k}\cdot \tag{23}$$

This coefficient takes into account the existence of ordered domains in the particle distribution. Outside the ordered region, the effective diffusion coefficient reduces to its ordinary definition,

$$D_{\rm eff}(p_k) = D(p_k, 0). \tag{23a}$$

In the case of a homogeneous disordered system, we recover the known expression [3],

$$\begin{aligned} D(p) \equiv D(p.0) &= a^2 w_0 {\rm e}^{-Kzp}(1 - Kzp(1-p)) \\ &= a^2 w_0 {\rm e}^{-Kzp}\left(1 + \frac{T_{\rm coex}}{T}\right) \end{aligned} \tag{24}$$

which is of the form [3],

$$D(p) = \Gamma(p) a^2 \left\{\partial(\mu/kT)/\partial \ln p\right\}_T \tag{25}$$

where $\Gamma(p)$ is the atomic jump rate; here

$$\Gamma(p) = w_0 {\rm e}^{-Kzp}(1-p).$$

The behaviour of the diffusion coefficient is shown in Figure 8 for various temperatures. We have arbitrarily chosen the energy E_0 in the activated jump probability of an isolated particle $w_0 = \nu_0 \exp(-E_0/kT)$ equal to $E_0 = -5\varepsilon$, in such a way that the various curves may be distinct but in a reasonable range. We notice here the abrupt variations of $D_{\rm eff}$ at the boundaries of the order-disorder transition. This reflects the fact that we used the equilibrium value for $\eta_{\rm eq}$. Close to the transition point, the jump is softened by dynamical finite size (finite gradients) effects which prevent η from relaxing to its equilibrium value. In particular, these finite gradient effects round the singular points of the phase diagram: we observe a dynamical phase diagram (Fig. 7).

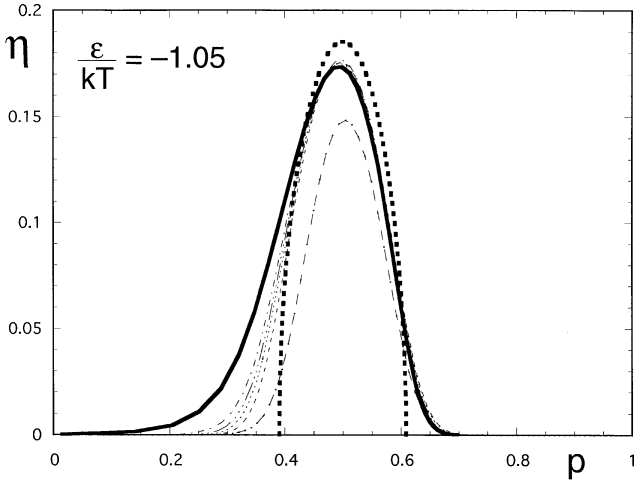

(a)

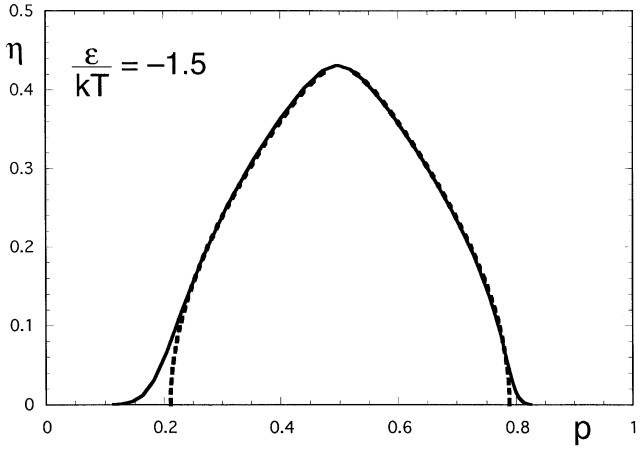

(b)

Fig. 7. Order parameter η from the resolution of equations (20, 21) in a system with fixed boundaries, for different times. (a) At $T/T_{\rm c}^{\rm MF} = 0.95$, (b) at $T/T_{\rm c}^{\rm MF} = 0.67$. The ordering is progressively established and becomes stable (solid curve). The curve $\eta(p)$ is rounded by finite size of the sample, leading to a dynamical phase diagram. The heavy dotted line corresponds to the static mean field diagram.

4.2 Scaling of the concentration profiles and corrections to the order parameter

Both for analytical considerations and for the numerical solution of the model it is convenient to consider open systems as well as closed fixed boundary systems which lead to stationary profiles. The concentration profile of an open system from Monte-Carlo simulations is shown in Figure 2, the dynamical mean field phase diagram resulting from the numerical solution of the equations (20) and (21) is plotted in Figures 7a and b, for two temperatures and different times. Interestingly, as time evolves there is first a deviation from the mean field diagram, before the system approaches the static curve with decreasing gradient. The plot for $p(x,t) = \pi(x/\sqrt{t})$ for the simulation data presented in Figure 3 shows how the scaling limit is approached: after a transitory period (up to roughly 16000 MCS in Fig. 3) the profile collapses toward

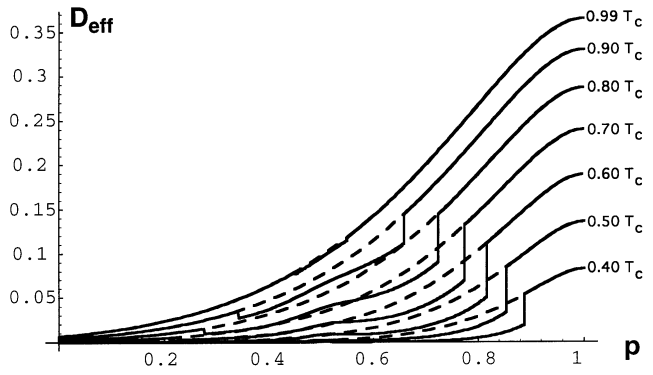

Fig. 8. Diffusion coefficient from the mean field equation for the evolution of the average concentration $p(x,t)$ and with $\eta = \eta_{\rm eq}(p)$ (Eq. (23)), as a function of concentration, for different temperatures T. $D_{\rm eff}$ has been multiplied by a factor $w_0 = \exp -5|\varepsilon|/T$ for graphical convenience. The dotted lines correspond to the $\eta = 0$ diffusion coefficient (unstable situation).

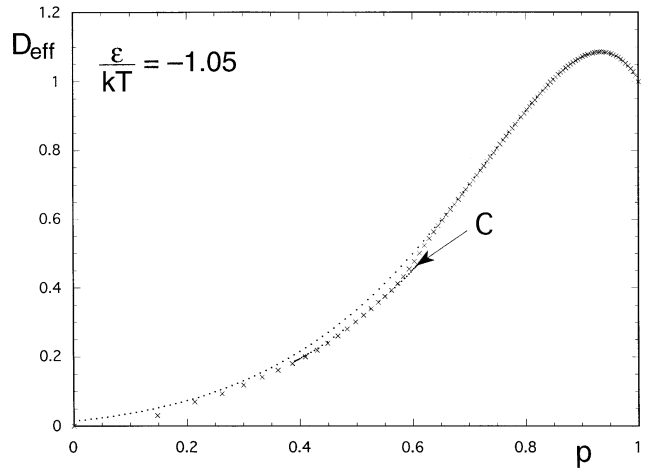

Fig. 9. Diffusion coefficient from direct simulations of the mean field equations, as a function of the concentration p. There is excellent agreement with the static approximation except near the transition points, where the (unphysical) jump shown by the points C (corresponding to the solution of Eq. (23)) is smoothed out.

a unique $\pi(x/\sqrt{t})$ profile over most of its domain. This evolution corresponds to the rapid relaxation of the order parameter due to the presence of the term of order zero, $\delta j \equiv \left\{ j_0^{\rm A}(k) - j_0^{\rm B}(k) \right\}$, in equation (21). Remember that the condition $\delta j = 0$, gives $\eta_k = \eta_{\rm eq}(p_k, T)$. When δj becomes small enough, the second order corrections on the right hand side of equation (21) become important; a scaling form $\eta(x,t) = \phi(x/\sqrt{t})$ is then appropriate. The Monte-Carlo simulations in Figure 4, and the numerical simulations of (20) and (21) in Figure 7, then show that $\eta(x,t)$ as a function of $p(x,t)$ reduces at long times to a simple function $\eta(p) = \eta(\pi[x/\sqrt{t}])$. In fact this function is not simply defined by the condition $\delta j = 0$, but by a condition which includes concentration gradients near the transition points. The evolution of $\eta(p, \Delta p)$ towards $\eta_{\rm eq}$ is then linked to the evolution of $\pi(x/\sqrt{t})$ towards a quasi-homogeneous profile (when $\nabla p \to 0$).

To sum up, we first observe that after a transitory regime, the ordered region extends to a much wider concentration range than expected by the statics.

4.3 The effective diffusion coefficient $D_{\rm eff}$

The preceding results also influence the effective diffusion coefficient. Equations (20, 21) remain valid if we replace $\eta_{\rm eq}(p)$ by the more general $\eta(p, \partial p/\partial x)$ taken from the above discussion. As equations (20, 21) are too complicated to be solved analytically the effective diffusion coefficient can only be obtained numerically. In Figures 5 we show a determination of $D_{\rm eff}$ from a calculation using the Monte-Carlo method, by applying Fick's law for each x value. Figure 9 shows $D_{\rm eff}$ using equations (20, 21) (crosses). The curve (C) indicates the modification of $D_{\rm eff}$ due to ordering using equation (23). We observe that the values are identical inside the ordered region, but that finite gradient effects are present around the critical concentrations $p_{c_1} \cong 0.4$ and $p_{c_2} \cong 0.6$ (in the long tail down to quite low concentrations).

5 Slow relaxation close to the phase transition points

The approach of the equilibrium is apparently very slow close to the two transition points p_{c_1} and p_{c_2}, as illustrated in Figures 7. In order to understand this behaviour, we look at the corrections to the asymptotic solutions $\eta = \eta_{\rm eq}(p)$ and $p = \pi(x/\sqrt{t})$ of equations (21, 22). The leading correction from the gradient term of equation (22) is of order $1/t$, with a coefficient that depends on $\eta_{\rm eq}$ and π. At sufficiently long times, the term becomes arbitrarily small, except close to the transition points, where the Laplacian of η dominates and diverges as $1/(\eta_{\rm eq}^3 t)$. Therefore the gradient term can no longer be treated as a small correction close to $p_{c_{1,2}}$. It has to be compared directly with the the dominant δj term, which behaves as η^3 resp. $\eta_{\rm eq}^3$. One concludes that the relaxation to equilibrium behaves as $\eta \cong t^{-1/6}$ near $p_{c_{1,2}}$. The range in η or in $\delta p \equiv |p - p_{\rm c}|$ over which this behaviour is valid will diminish with time, the crossover values evolving as $\eta_x \cong t^{-1/6}$ resp. $\delta p_x \equiv |p - p_{\rm c}| \cong t^{-1/3}$. For the gradient term $\nabla\eta$ we conclude that it relaxes at the critical points despite the ordering, but at a slower rate, $\nabla\eta \cong \delta\eta/\delta p \nabla p \cong t^{-1/3}$ instead of $\nabla\eta \cong t^{-1/2}$ far from the transitions.

In Figure 10, the maximum value of $\mathrm{d}\eta/\mathrm{d}x$ (which is sharply peaked close to the transitions) is shown as a function of time for $T/T_{\rm c} = 0.71$. It can be fitted very well by a power law with an exponent $-1/3$. Similarly, the value of η at the transitions, $p_{c_1} = 0.2327$ and $p_{c_2} = 0.7673$, has been measured as a function of time; it decreases with the predicted exponent $-1/6$.

Finally, we postulate that the correction to the asymptotic form for η should have the following scaling form,

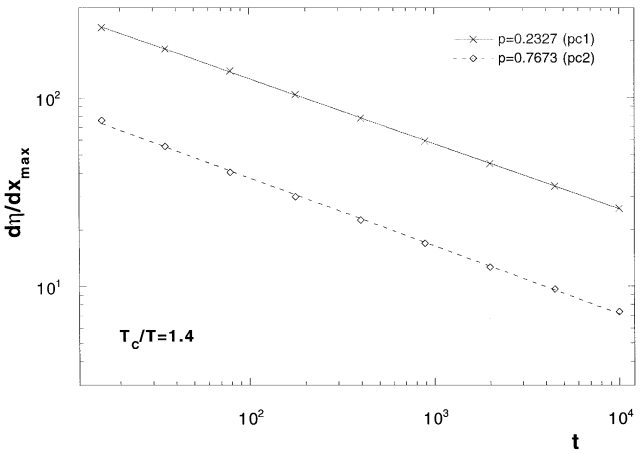

Fig. 10. Evolution of the gradient $\nabla\eta/\nabla x$ near the transition points, $p_{c_1} = 0.2327$ and $p_{c_2} = 0.7673$ at $T/T_c = 0.71$. The maximum of the gradient at the lower ($\times$) respectively the upper ($\Diamond$) transition is plotted against time, on a log-log scale. Both data sets fit a power law with an exponent -0.34 ± 0.02, consistent with the theoretical prediction $-1/3$.

for $t \to \infty$ and $\delta p \equiv |p - p_c| \to 0$,

$$\eta(x,t) - \eta_{eq}(\pi(x/\sqrt{t})) = t^{-1/6}\varphi_{\pm}(\delta p\ t^{1/3}) \qquad (26)$$

$\varphi_{\pm}$ being the scaling functions below and above the transition.

To check this form, we have plotted $(\eta - \eta_{eq})\ t^{1/6}$ against $\delta p\ t^{1/3}$ in Figure 11, for the upper transition. The data fits the scaling form remarkably well, even for times as short as $t = 15$. A similar behaviour is observed for the lower transition. Note that φ crosses the origin, which means that the asymptotic form is approached from different sides depending on δp.

The kinetic equation of the order parameter, equation (21), therefore suggests the following overall behaviour of η: at very short times the evolution of η is driven by the dominant term

$$-z(j_0^A(k) - j_0^B(k));$$

after this initial transitory period, the evolution of η is determined by the finite gradient effects and by the boundary condition. For an open system, the concentration profile evolves towards a quasi homogeneous distribution, and $\eta(p)$ approaches $\eta_{eq}(p)$. In a finite size system of size L with a source at an extremity and a sink at the other extremity, $\eta(p)$ reaches a smoothed curve $\eta_L(p)$, which approaches $\eta_{eq}(p)$ for $L \to \infty$. At late times, the dominant contribution is given explicitly by the term

$$G(p_k, \eta_k)\Delta_a\eta_k$$

in equation (21), near the critical concentrations p_{c_1} and p_{c_2}. The leading time evolution of η can therefore be described by the equation

$$\frac{\partial \eta_k}{\partial t} = -z\left(j_0^A(k) - j_0^B(k)\right) + G(p_k, \eta_k)\Delta_a\eta_k. \qquad (27)$$

6 Conclusion

We conclude that the mean field approximation captures the main features of the diffusion in presence of ordering due to repulsive nearest neighbour interactions. The comparison between static and dynamic mean field approximations and Monte-Carlo simulations show that there are significant effects near the transition points, whereas inside the ordered domains respectively far into the homogeneous domains there is excellent agreement between static and dynamic. However, inside the ordered domains the presence of domain boundaries, along which the diffusion is easier, leads to a higher diffusion coefficient than one would expect on the basis of the argument, that the ordering prevents diffusion. Only at low temperature, the diffusion may be affected by the very low diffusivity through the ordered structures.

A discontinuity in the diffusion coefficient as a function of the concentration is found in first approximation near the order-disorder transition lines, which is softened when the finite gradients are included as shown in Figure 9. There is a very slow convergence, as the concentration gradients go to zero, towards the limiting behaviour near the transitions: a discontinuity of the diffusion coefficient. Therefore — within the mean-field approximation - the concentration profile $p(x)$ presents discontinuities of its gradient $\mathrm{d}p/\mathrm{d}x$, in the limit of vanishing gradients. Far from the homogeneous limit, the profile $p(x)$ are softened around the points p_{c_1} and p_{c_2} in a range δp scaling like $t^{-1/3}$ corresponding to a spatial range δx scaling like $t^{1/6}$.

No such effect can be observed in the Monte-Carlo simulations. This may be due to the fluctuations, the relatively short time scales (the mean field calculations are ten times longer and the effects only appear at the latest times) and the true, *i.e.* non-classical, transition.

Appendix A: The mean-field approach

In the mean-field approximation, all the operators n_k in the expressions for the jump probabilities $w_{k,k+a}$ are replaced by their average concentrations p_k. Depending on the explicit form of the jump operators, different approximations can be obtained.

The general expression for the current can then be written,

$$J_{ij}^{AB}(\{p\}) = w_0 \left\{ \prod_{a'} w_r(p_{i+a'}^B) p_i^A (1 - p_j^B) - \prod_{a'} w_r(p_{j+a'}^A) p_j^B (1 - p_i^A) \right\} \qquad (A.1)$$

where $w_r(p_i^A) = \langle \exp -\frac{\varepsilon}{kT} n_i^A \rangle$ is the contribution of the occupation of site i to the jump probability. A similar expression is obtained for $J_{ji}^{BA}(\{p\})$.

As already noticed above, we will take the average in the exponential for w_r; this average leads to the usual

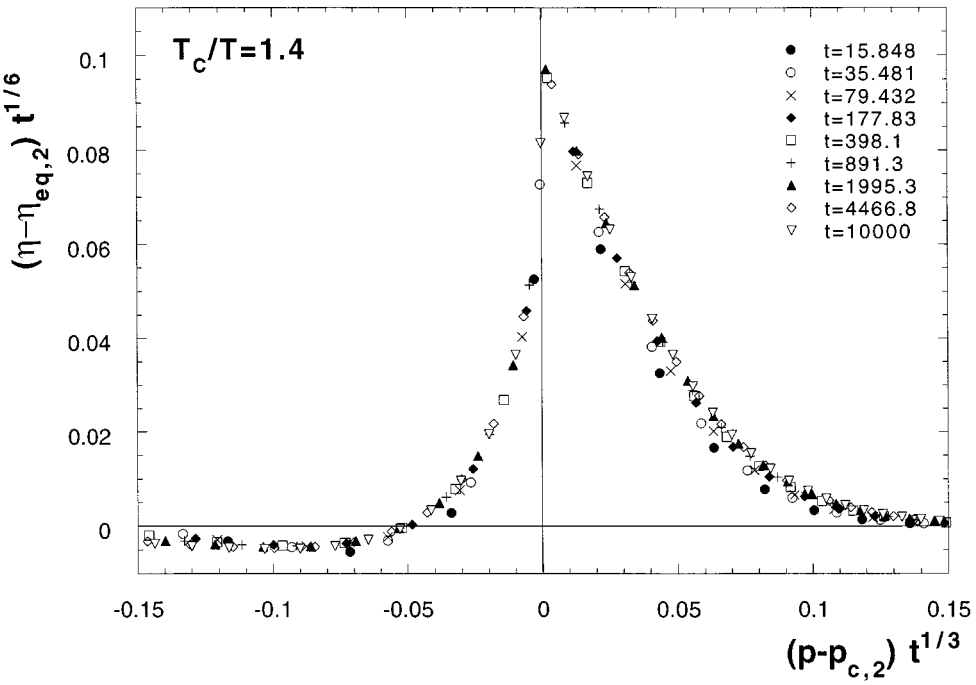

Fig. 11. Scaling function of $\eta(x,t)$ near the upper transition. $t^{1/6}$ $(\eta(x,t) - \eta_{\rm eq}(p(x,t)))$ is plotted against $t^{1/3}\delta p$ at times ranging between $t = 15$ to $t = 10\,000$. The data collapse very well on a single curve, both below and above the transition.

thermodynamic equilibrium:

$$w_{\rm r}(p_i^{\rm A}) = \exp -\frac{\varepsilon}{kT} p_i^{\rm A}. \tag{A.2}$$

To introduce conveniently the thermodynamic variables one can proceed as in reference [20], factorizing the currents into a contribution S, symmetrical with respect to the initial and final state, and a factor which is the difference between a local function C invariant under the transformations of the local symmetry point group, taken at the final j and initial i states,

$$J_{ij}^{\rm AB}(\{p\}) = -S_{ij}^{\rm AB}(C_j^{\rm B} - C_i^{\rm A}). \tag{A.3}$$

This equation, together with the equations of evolution of the concentrations (9, 10), leads to generalized Allen-Cahn equations [19].

After identification one finds (up to an arbitrary constant factor c_0),

$$C_i^{\rm A} = c_0 \frac{p_i^{\rm A}}{1 - p_i^{\rm A}} \prod_{a'} w_{\rm r}(p_{i+a'}^{\rm B}) \tag{A.3a}$$

$$S_{ij}^{\rm AB} = \frac{w_0}{c_0}(1 - p_i^{\rm A})(1 - p_j^{\rm B}). \tag{A.3b}$$

From (A.3a) it is possible to introduce what can be identified to be a chemical potential on each site $\{i, {\rm A}\}$ or $\{j, {\rm B}\}$,

$$\mu_i^{\rm A} = kT \log C_i^{\rm A} \quad \text{and} \quad \mu_j^{\rm B} = kT \log C_j^{\rm B} \tag{A.4}$$

defined *via* equations (A.2) and (A.3a) (c_0 has been chosen here such that $\mu_{k_0} \Longrightarrow -\mu_{k_0}$ when $p_k \Longrightarrow 1 - p_k$) by,

$$\begin{aligned} \mu_k^{\rm A} &= \mu_{k_0}^{\rm A} \\ &\equiv -z\varepsilon \left(p_k^{\rm B} - \frac{1}{2}\right) - \varepsilon \sum_{a'} \mathcal{D}_{a'} p_k^{\rm B} + kT \log \frac{p_k^{\rm A}}{1 - p_k^{\rm A}} \end{aligned} \tag{A.4a}$$

$$\begin{aligned} \mu_k^{\rm B} &= \mu_{k_0}^{\rm B} \\ &\equiv -z\varepsilon \left(p_k^{\rm A} - \frac{1}{2}\right) - \varepsilon \sum_{a'} \mathcal{D}_{a'} p_k^{\rm A} + kT \log \frac{p_k^{\rm B}}{1 - p_k^{\rm B}} \cdot \end{aligned} \tag{A.4b}$$

The quantities $C^{\rm A}$ and $C^{\rm B}$ are equivalent to *absolute activities* [16]. Expressions (A.4) derived directly from the master equations (9, 10), can also be obtained as the extremum of a free energy $\langle F \rangle$ with the constraint of a fixed number of particles, $\delta \left\{ \langle F \rangle - \mu_1 \left(\sum_i p_i^{\rm A} + \sum_j p_j^{\rm B} \right) \right\} = 0$, giving at equilibrium,

$$\mu_1 = \frac{\partial \langle F \rangle}{\partial p_i^{\rm A}} = \mu_{i_0}^{\rm A} - \mu_{\rm e} - \frac{z}{2}\varepsilon = \frac{\partial \langle F \rangle}{\partial p_j^{\rm B}} = \mu_{j_0}^{\rm B} - \mu_{\rm e} - \frac{z}{2}\varepsilon$$

with a free energy,

$$\langle F\rangle = F_+ \sum_{i\in\{\mathrm{A}\}}\left(-\frac{\varepsilon}{2}\sum_a p_i^{\mathrm{A}}p_{i+a}^{\mathrm{B}} - \mu_{\mathrm{e}}p_i^{\mathrm{A}} + kT(p_i^{\mathrm{A}}\ln p_i^{\mathrm{A}} + (1-p_i^{\mathrm{A}})\ln(1-p_j^{\mathrm{B}}))\right) \times \sum_{j\in\{\mathrm{B}\}}\left(-\frac{\varepsilon}{2}\sum_a p_j^{\mathrm{B}}p_{j+a}^{\mathrm{A}} - \mu_{\mathrm{e}}p_j^{\mathrm{B}} + kT(p_j^{\mathrm{B}}\ln p_j^{\mathrm{B}} + (1-p_j^{\mathrm{B}})\ln(1-p_j^{\mathrm{B}}))\right). \quad (A.5)$$

The symmetry between particles and holes, leading to relations (A.4), can be made visible by taking advantage of the arbitrariness (choice of the zero of energies) of μ_{e} (or of c_0): $\mu_{\mathrm{e}} = kT\log c_0 = -\frac{z}{2}\varepsilon$ so that at equilibrium,

$$\mu_1 = \frac{\partial\langle F\rangle}{\partial p_i^{\mathrm{A}}} \equiv \mu_{i0}^{\mathrm{A}} = \frac{\partial\langle F\rangle}{\partial p_j^{\mathrm{B}}} \equiv \mu_{j0}^{\mathrm{B}}. \quad (A.5a)$$

Using SES, we now choose a situation with concentrations p_k^{A} and p_k^{B} defined on each site k, and initially *slowly varying in space*. Introducing $\Delta F = 2\{\langle F\rangle - F_0\}$ as a sum over *all* lattice sites k,

$$\Delta F = -\varepsilon\sum_{k,a} p_k^{\mathrm{A}}p_{k+a}^{\mathrm{B}} + \sum_k\left(-\mu_{\mathrm{e}}p_k^{\mathrm{A}} + kT\left(p_k^{\mathrm{A}}\ln p_k^{\mathrm{A}} + (1-p_k^{\mathrm{A}})\ln(1-p_k^{\mathrm{A}})\right)\right) + \sum_k\left(-\mu_{\mathrm{e}}p_k^{\mathrm{B}} + kT\left(p_k^{\mathrm{B}}\ln p_k^{\mathrm{B}} + (1-p_k^{\mathrm{B}})\ln(1-p_k^{\mathrm{B}})\right)\right). \quad (A.5b)$$

From relation (A.4), the current (Eq. (A.3)) can be written in a generalized Cahn-Hilliard form, a

$$J_{ij}^{\mathrm{AB}}(\{p\}) = -M_{ij}^{\mathrm{AB}}(\mu_j^{\mathrm{B}} - \mu_i^{\mathrm{A}}) \quad (A.6a)$$

with a mobility M, given in first approximation (by linearization of Eq. (A.3) the small parameter being $\Delta\mu = \mu_j^{\mathrm{B}} - \mu_i^{\mathrm{A}}$, and with all p's replaced by their equilibrium values) by,

$$M_{ij}^{\mathrm{AB}}(\{p\}) \cong \beta S_{ij}^{\mathrm{AB}}\sqrt{C_i^{\mathrm{A}}C_j^{\mathrm{B}}}. \quad (A.6b)$$

Far from equilibrium, the corrections due to the non homogeneous chemical potential are implicitly included in the mobility (using Eqs. (A.3, A.4, A.6a), see also Eq. (12c) of Ref. [20]).

Appendix B: The order-disorder transition

The mean-field phase diagram can be obtained by setting the currents to zero (Eq. (A.1)), in an homogeneous medium:

$$p_i^{\mathrm{A}} \equiv p^{\mathrm{A}} \text{ and } p_j^{\mathrm{B}} \equiv p^{\mathrm{B}} \text{ for any } i \text{ and } j,$$

and by fixing (using (A.1, A.3)) the chemical potentials, associated with a given temperature T and a fixed *average* concentration p_0:

$$\mu_i^{\mathrm{A}} \equiv \mu_j^{\mathrm{B}} \equiv \mu_m \text{ for any } i \text{ and } j.$$

It is more suitable to change the variables and to introduce, using the SES approach, the average concentration p_k and the order parameter η_k:

$$p_k \equiv \frac{p_k^{\mathrm{A}} + p_k^{\mathrm{B}}}{2},\ \eta_k \equiv \frac{p_k^{\mathrm{A}} - p_k^{\mathrm{B}}}{2}\cdot \quad (B.1)$$

The phase diagram is defined starting from equation (A.4) with, $p_k \equiv p = (p^{\mathrm{A}}+p^{\mathrm{B}})/2$, and $\eta_k \equiv \eta = (p^{\mathrm{A}}-p^{\mathrm{B}})/2 = 0$, that is to say by the equation,

$$-z\varepsilon p^{\mathrm{B}} + kT\log\frac{p^{\mathrm{A}}}{1-p^{\mathrm{A}}} = -z\varepsilon p^{\mathrm{A}} + kT\log\frac{p^{\mathrm{B}}}{1-p^{\mathrm{B}}}\cdot \quad (B.2)$$

This equation is conveniently solved by considering the function,

$$f(u) = z\varepsilon\left(u - \frac{1}{2}\right) + kT\log\frac{u}{1-u} \quad (B.3)$$

related to the chemical potentials of homogeneous concentrations by

$$\mu^{\mathrm{A}} = f(p^{\mathrm{A}}) - 2z\varepsilon\left(p - \frac{1}{2}\right) \quad (B.4a)$$

$$\mu^{\mathrm{B}} = f(p^{\mathrm{B}}) - 2z\varepsilon\left(p - \frac{1}{2}\right) \quad (B.4b)$$

so that (B.2) becomes

$$f(p^{\mathrm{A}}) = f(p^{\mathrm{B}}). \quad (B.5)$$

Using equation (A.4), this defines an equation for p and η. The corresponding phase diagram is shown in Figure 6. The diagram is symmetrical with respect to $p = 1/2$; the critical mean-field temperature is $kT_{\mathrm{c}}^{\mathrm{MF}} = -z\varepsilon/4$.

At equilibrium the temperature is then a function of p and η given by the equation (solving (B.3) and (B.5)),

$$kT(p,\eta) = -\frac{2\varepsilon z\eta}{\log\left(1 - \frac{2\eta}{(p-\frac{1}{2})^2 - (\eta-\frac{1}{2})^2}\right)}\cdot \quad (B.6)$$

The coexistence curve is then simply given by the $\eta = 0$ limit,

$$kT(p,0) = -\varepsilon z p(1-p). \quad (B.7)$$

Needless to say that the mean field phase diagram only gives a qualitative idea of the true phase diagram, especially near the transition. The latter has for instance been estimated by Binder and Landau [24] by Monte-Carlo calculations.

References

1. *Physics of Superionic Conductors*, edited by M.B. Salamon (Springer-Verlag, Berlin, 1979); Proc. of the 6th Int. Conf. on Solid State Ionics, Garmish 1987, Solid State Ionics **28-30** (1988); Proc. of the 11^{th} international symposium, Princeton University (June 1988), Solid State Ionics **32-33** (March 1989).
2. G. Betz, H. Tributsch, Progress in Solid State Chemistry **16** 195-290 (1985); A.D. Yoffe, Solid State Ionics **9-10**, 59-69 (1983).
3. D.A. Reed, G. Ehrlich, Surf. Sci. **102**, 588 (1981).
4. C. Cohen, Y. Girard, P. Leroux-Hugon, A. L'Hoir, J. Moulin, D. Schmaus, Europhys. Lett. **24**, 767 (1993).
5. G. Nicolis, I. Prigogine, *Self-Organization in Non-Equilibrium Systems* (Wiley Interscience, New York, 1977); H. Haken, *Synergetics* (Springer-Verlag, New York, 1983); S.W. Koch, *Dynamics of First Order Phase Transitions in Equilibrium and Non-Equilibrium Systems* (Springer-Verlag, Berlin, 1984).
6. A. Natori, H. Ohtsubo, Surf. Sci. **184**, 289 (1987).
7. A. Sadik, K. Binder, Surf. Sci. **128**, 350 (1983).
8. A.A. Tarasenko and A.A. Chumak, Sov. Phys. Solid State **22** 1716 (1980); **24**, 1683 (1982).
9. C. Uebing, R. Gomer, J. Chem. Phys. **95**, 762 (1991).
10. M. O'Keeffe, Comments on Solid State Physics **7**, 63 (1977).
11. Y. Boughaleb, J.F. Gouyet, Solid State Ionics **9-10**, 1401 (1983).
12. A.J. Berlinsky, W.G. Unruh, W.R. McKinnon, R.R. Haering, Solid State Communications **31**, 135 (1979); Y. Chab, P. Deniard, in *Chemical Physics of Intercalation*, edited by A.P. Legrand, S. Flandrais, NATO ASI Series **B 172**, 395 (1987).
13. C. John Wen, B.A. Boukamp, R.A. Huggins, J. Electrochem. Soc. **126**, 2258 (1979).
14. H. Sato, R. Kikuchi, J. Chem. Phys. **55**, 677 (1971); R. Kikuchi, H. Sato, J. Chem. Phys. **55**, 702 (1971).
15. G.E. Murch, R.J. Thorn, Philos. Mag. **35**, 493 (1977); G.E. Murch, Philos. Mag. A **43**, 871 (1981).
16. W. Dieterich, J. Stat. Phys. **39**, 583 (1894). references therein.
17. L. Boltzmann, Ann. Physik **53**, 959 (1894).
18. C. Matano, Jap. J. Phys. **8**, 109 (1933).
19. J.-F. Gouyet, Phys. Rev. E **51**, 1695 (1995).
20. J.-F. Gouyet, Europhys. Lett. **21**, 335 (1993).
21. K.R. Subbaswamy, G.D. Mahan, Phys. Rev. Lett. **37**, 642 (1976).
22. *Applications of the Monte-Carlo Method in Statistical Physics*, Topics in Current Physics, edited by K. Binder, (Springer Verlag, Berlin Heidelberg 1987).
23. A factor 1/2 was missing in equations (37, 38, 40), and $-1/2$ in equation (39), of reference [19].
24. K. Binder, D.P. Landau, Phys. Rev. B **21**, 1941 (1980).